Macromolecules

Article

pubs.acs.org/Macromolecules

Structure Optimization and Mechanical Model for Microgel-Reinforced Hydrogels with High Strength and Toughness

Jian Hu,[†] Takayuki Kurokawa,[‡,§] Kenta Hiwatashi,[†] Tasuku Nakajima,[‡] Zi Liang Wu,[†] Song Miao Liang,[‡] and Jian Ping Gong*[,‡,§]

[†]Graduate School of Science, Hokkaido University, Sapporo 060-0810, Japan

[‡]Faculty of Advanced Life Science, Hokkaido University, Sapporo 060-0810, Japan

[§]Creative Research Institution, Hokkaido University, Sapporo 001-0021, Japan

Supporting Information

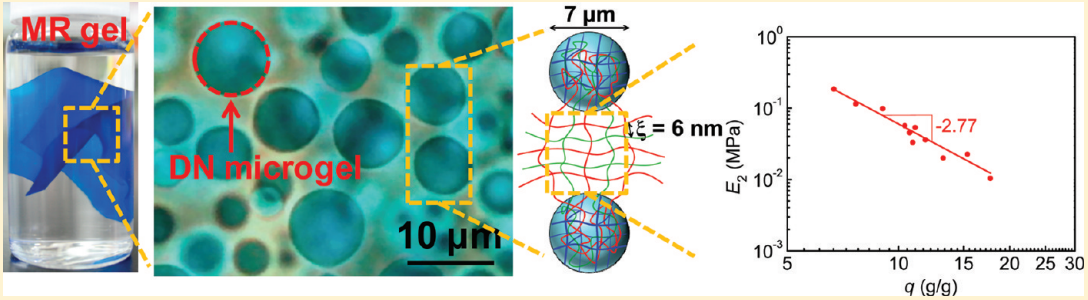

ABSTRACT: In this work, the mechanical behavior of sparsely cross-linked, neutral polyacrylamide (PAAm) hydrogels containing densely cross-linked polyelectrolyte microgels of poly(2-acrylamido-2-methylpropanesulfonic sodium) (PNaAMPS) were studied systematically by varying the formulations. The microgel-reinforced (MR) hydrogels have a two-phase composite structure, where the disperse phase is the *rigid* double-network (DN) microgels, and the continuous phase is the *soft* PAAm matrix. At the optimal formulation, the MR gels showed high mechanical strength and toughness, comparable to conventional DN hydrogels. The two critical parameters for the substantial enhancement of mechanical strength and toughness of MR gels are the concentration of PNaAMPS microgel and the molar ratio of the PAAm to the PNaAMPS in the microgel phase. Selective dyeing of the embedded microgels in MR gels allowed for visualization of the deformation of microgels, and we found that the local strain of microgels was much smaller than the global strain applied on MR gels; this indicates that isostress model (Reuss's model) is more suitable than isostrain model (Voigt's model) for this composite system.

I. INTRODUCTION

Hydrogels have drawn great attention for their potential biomedical applications such as drug carriers,[1] extracellular matrices,[2] and artificial soft tissues.[3] However, the low mechanical strength of hydrogels has been a significant disadvantage, posing difficulties in many load-bearing applications. Over the past decade, several mechanically robust hydrogels with different network topologies have been developed, such as double-network (DN) hydrogels,[4] slide-ring (SR) hydrogels,[5] and nanocomposite (NC) hydrogels.[6] Many studies based on or inspired from these robust hydrogels have been reported recently.[7−11] Several recent review articles have described the development of hydrogels with high mechanical strength.[12−16]

To date, DN hydrogels are the toughest synthetic hydrogels, with fracture energy close to some rubbers.[15] The extensive studies on the toughening mechanism of DN gels have shown that yielding and large hysteresis exist for tensile deformation, and a large damage zone is formed at the crack tip, which effectively avoids the stress concentration and increases the resistance against the crack propagation.[17−19] The nonelastic behaviors of DN gels are associated with the fracture of the rigid and brittle polyelectrolyte network, which indicates that the brittle component serves as *sacrificial bonds* in the toughening of DN gels.

We assume, from the toughening mechanism of DN gels, that introduction of any effective *sacrificial bonds* that yield and dissipate energy upon deformation will toughen the materials. On the basis of this assumption, we have introduced various motifs of sacrificial bonds into hydrogels.[20−22] One successful approach that was recently found to toughen soft polyacrylamide (PAAm) gels dramatically was incorporating densely cross-linked microgels into the gels.[20,21] The precise definition of microgel by IUPAC is a "particle of gel of any shape with an equivalent diameter of approximately 0.1−100 μm".[23] Recently, the reinforcement effect of microgels in hydrogel matrices have been reported in several other hydrogel systems.[24−27] In our system, the microgel-reinforced hydrogels,

Received: February 22, 2012
Revised: May 26, 2012
Published: June 5, 2012

Scheme 1. Procedure for Synthesizing Microgel-Reinforced (MR) Hydrogels by Two-Step UV Polymerization of AAm Solution (Revised from the Literature[21])

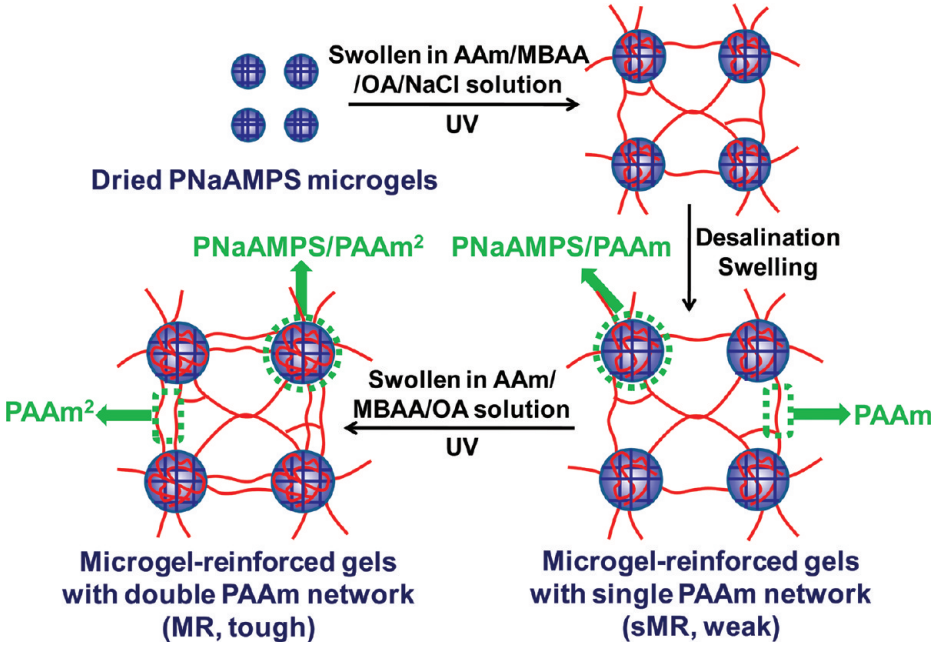

named as MR hydrogels, have a distinctive two-phase composite structure where the disperse phase is *rigid* double-network (DN) microgels and the continuous phase is the sparsely cross-linked *soft* PAAm matrix. We have preliminarily confirmed that the high mechanical strength and toughness of MR gels root in the fracture of the microgels during deformation, similar to the sacrificial bonds mechanism of DN gels. In this work, we first systematically explored the effects of synthesis formulations, including the concentrations of microgels $C_{microgel}$, sodium chloride C_{NaCl}, AAm monomer for the first network C_{AAm1}, MBAA cross-linker for the first network C_{MBAA1}, and AAm monomer for the second network C_{AAm2}, on the mechanical properties of MR gels. As a result, we have found that the microgel concentration and the molar ratio of the PAAm to the PNaAMPS in the microgel phase are the two critical parameters for the substantial enhancement of mechanical strength and toughness of MR gels. We then studied the correlation between the local deformation of microgels and the global deformation of MR gels, taking the advantage of the direct visualization of the embedded microgels in MR gels. On the basis of these results, we discussed the appropriate mechanical model to describe the mechanical behaviors of the MR gel system. Finally, we gave a two-phase composite picture for MR gels from structural and mechanical viewpoints.

II. EXPERIMENTAL SECTION

Materials. The monomer, 2-acrylamido-2-methylpropanesulfonic sodium (NaAMPS) (Tokyo Kasei Co., Ltd.) was used as received. The cross-linker, *N*,*N*′-methylenebis(acrylamide) (MBAA) (Tokyo Kasei Co., Ltd.) was recrystallized from ethanol. The monomer, acrylamide (AAm) (Junsei Chemical Co., Ltd.) was recrystallized from chloroform. The UV initiator, 2-oxoglutaric acid (OA) (Wako Pure Chemical Industries, Ltd.) was used as received. The surfactant, polyglycerol polyricinoleate (PGPR) (Danisco Co., Ltd.) was used as received. The solvent, kerosene (Wako Pure Chemical Industries, Ltd.) was used as received. The dye, alcian Blue (Wako Pure Chemical Industries, Ltd.) was used as received. Milli-Q (18.3 MΩ) water was used in all experiments.

Synthesis. *Preparation of Microgels.* Similar to our previous work, poly(2-acrylamido-2-methylpropanesulfonic sodium) (PNaAMPS) microgels were prepared by SPG (Shirasu Porous Glass) membrane emulsification and UV polymerization.[21] First, water/oil (W/O) emulsion was prepared by high-speed mini kit equipped with a hydrophobic SPG membrane (SPG Technology Co., Ltd.). The disperse phase was an aqueous solution of 1 M NaAMPS containing 4 mol % cross-linker MBAA and 0.1 mol % UV initiator OA, with respect to NaAMPS monomer. The disperse phase, stored in a pressure-tight vessel, was pressed into the continuous phase, kerosene containing 1 wt % surfactant PGPR, through the hydrophobic SPG membrane (pore diameter = 4.9 μm) under argon transmembrane pressure of 14 kPa. After bubbling with argon for 1 h, the W/O emulsion was irradiated at 365 nm UV with intensity of 4 mW/cm^2 under an argon atmosphere for 8 h. This led to the polymerized PNaAMPS microgels. To purify the microgels, they were precipitated with acetone to remove the surfactant, then reswollen in deionized water to remove the residual monomers, and finally separated by ultracentrifugation at 10^4 rpm, 3 times. After freeze-drying, the dried PNaAMPS microgels were obtained as fine powders.

Preparation of MR Hydrogels. The procedure for preparing MR hydrogels was described as our previous work.[21] As shown in Scheme 1, *dried* PNaAMPS microgel powders ($C_{microgel}$, g/mL) were swollen in the first aqueous precursor solution (1 mL) containing AAm (C_{AAm1}, M), MBAA (C_{MBAA1}, mol %), 0.01 mol % OA, and sodium chloride (C_{NaCl}, M); here mol % was related to AAm monomer concentration. The NaCl was used to control the solution at a suitable operating viscosity, and a high C_{NaCl} was used for a high $C_{microgel}$. After equilibrium swelling, the paste-like solution was poured into a mold consisting of a 100 μm silicone spacer sandwiched by two parallel glass plates and then polymerized under an argon atmosphere with UV irradiation for 8 h. The as-prepared hydrogels were desalinated completely in deionized water and were denoted as sMR gels for their single PAAm network structure. Then the sMR gels were swollen in the second aqueous precursor solution of AAm with a concentration (C_{AAm2}, M) containing 0.01 mol % MBAA and 0.01 mol % OA. After equilibrium swelling, the sMR gels were covered by two parallel glass plates and wrapped by plastic film and then irradiated with UV under an argon atmosphere for 8 h. Finally, the gels were swollen in

dx.doi.org/10.1021/ma3003664 | *Macromolecules* 2012, 45, 5218−5228

sMR gels: $C_{microgel}$-C_{NaCl}-(C_{AAm1}-C_{MBAA1}) g/mL-M-(M-mol%)

MR gels: $C_{microgel}$-C_{NaCl}-(C_{AAm1}-C_{MBAA1})-C_{AAm2} g/mL-M-(M-mol%)-M

deionized water to remove the residual chemicals, and the tough MR gels with two interpenetrating PAAm networks were obtained. As a reference, a pure PAAm gel without adding any microgels was also prepared by the two-step sequential polymerization as above. Correspondingly, PAAm and $PAAm^2$ represented the PAAm gel with a single network and double network, respectively. In this paper, all the sMR and MR gels were coded according to their compositions, and the sample nomenclature was shown as follows:

Selective Dyeing of MR Gels. MR gels were immersed in 3 vol % acetic acid aqueous solution containing 1 wt % Alcian Blue for 15 min and then washed in deionized water. The tetravalent cationic Alcian Blue dyes the anionic PNaAMPS microgels, but not the neutral PAAm matrix, which produces a sharp contrast between the microgel phase and the matrix phase in favor of the observation of microgels under an optical microscope.

Preparation of DN Hydrogels. DN hydrogel films were prepared as the method described in our previous work.[28] With the same composition as the NaAMPS solution for synthesizing PNaAMPS microgels, an aqueous solution of 1 M NaAMPS monomer containing 4 mol % MBAA and 0.1 mol % OA was poured into a mold consisting of a 100 μm silicone spacer sandwiched by two parallel glass plates and then polymerized with UV lamps for 8 h to obtain PNaAMPS gels. The PNaAMPS gels were swollen in the first aqueous solution of 2 M AAm containing 0.01 mol % MBAA, 0.01 mol % OA, and 0.1 M NaCl. Here the presence of NaCl prevented the PNaAMPS gels from dramatic swelling to facilitate the operation. Then the partial-swollen PNaAMPS gels were polymerized with UV lamps for 8 h. These prereinforced gels, sDN gels (only a single PAAm network), were desalinated completely in deionized water. Then the sDN gels were swollen to equilibrium in the second aqueous solution of 2 M AAm containing 0.01 mol % MBAA and 0.01 mol % OA, and polymerized with UV lamps for 8 h. After equilibrium swelling, tough DN gels were obtained.

We assume that the sDN and DN gels thus prepared possessed the similar chemical compositions to the PNaAMPS/PAAm microgels embedded in the sMR gels and the PNaAMPS/$PAAm^2$ microgels embedded in the MR gels (Scheme 1), respectively. Accordingly, the mechanical behaviors of the embedded microgels in sMR and MR gels can be approximately simulated by sDN and DN gels, respectively.

Characterizations. *Size Distribution of Microgels.* To characterize the size of the PNaAMPS microgels in various conditions, their micrographs were captured under the differential interference contrast microscope (DIC; Olympus BX50). The size distribution of the microgels was determined by statistically measuring the diameter of 300 microgels in the captured DIC images with the analytic software, Image-Pro Plus. The frequency of microgels is defined as the number percentage of the 300 microgels. To evaluate the dispersity of the microgels quantitatively, the coefficient of variation is defined as $CV = (SD/D_m) \times 100\%$, where SD is the standard deviation of the microgel diameters and D_m is the number-average mean microgel diameter. In general, the case of CV below 10% is considered as monodisperse.[29]

Turbidity. The apparent absorbance, A, of hydrogels was measured at a wavelength of 550 nm, at room temperature, by a model 680XR plate reader (Bio-Rad). To calculate A, five different spots on one sample were taken and averaged. In order to compare the transparency among samples of different thickness, we calculated the turbidity, τ, of all the samples assuming that τ is uniform for the samples, $\tau = A/w$, where w is the thickness of the samples measured under an optical microscope.[30] The τ obtained is the intrinsic parameter related to the absorption coefficient and the scattering coefficient.

Equilibrium Swelling Ratio. The equilibrium swelling ratio q is defined as $q = W_{eq}/W_{dry}$, where W_{eq} and W_{dry} are the weight of hydrogels in the fully swollen state and dry state, respectively.

Volume Expansion Ratio. During the preparation of MR gels, the side length of the square-shaped gels were recorded as L_0, L_1, and L_2, for as-prepared sMR gels, swollen sMR gels, and swollen MR gels, respectively. The volume expansion ratio Q for sMR and MR gels are defined as $(L_1/L_0)^3$ and $(L_2/L_1)^3$, respectively.

Volume Fraction of Microgels. For the traditional rubber/carbon black composites,[31] as well as the poly(dimethylacrylamide)/silica hybrid hydrogels,[32] the volume fraction of the solid fillers can be estimated easily from their formulations in feed. However, in the system of sMR or MR gels, we could not estimate the volume fraction of the microgels from the weight of the dry microgel powders added to the precursor solutions, considering the swelling of the microgel phase and the matrix phase, as well as the influence of NaCl. Consequently, we attempted to estimate the volume fraction ϕ_1 of microgels from the two-dimensional DIC images of the samples by image analysis. The total cross-section area A_t of microgels in one DIC image of size $L \times L$ is

$$A_t = \pi R_m^2 n^2 \tag{1}$$

where R_m and n^2 are the mean radius of microgels and the number of microgels per DIC image. Assuming that all the microgels distribute in the three-dimensional PAAm matrix uniformly, the total volume of the microgels in volume L^3 is

$$V_t = \frac{4}{3}\pi R_m^3 n^3 \tag{2}$$

From the above relations, the volume fraction ϕ_1 of microgels is derived as follows:

$$\phi_1 = \frac{V_t}{L^3} = \frac{4}{3L^3}\sqrt{\frac{A_t^3}{\pi}} \tag{3}$$

Therefore, we measured the total cross-sectional area A_t of microgels in one designated DIC image area L^2 of 80.86 × 80.86 μm^2, and estimated the microgel volume fraction ϕ_1 for each sample. Since L is much larger than R_m, and n^2 is more than 50 in each DIC image, this method gives enough accuracy to ϕ_1.

Tensile Properties. Tensile test was performed with a commercial test machine (Tensilon RTC-1150A, Orientec Co.). The fully swollen samples were cut into a dumbbell shape as standardized JIS-K6251-7 sizes (length 35 mm, width 2 mm, gauge length 12 mm) with a gel cutting machine (DumbBell Co., Ltd.). Both ends of the dumbbell-shaped samples were clamped and stretched at a constant velocity of 100 mm/min. The fracture stress σ_b and fracture strain ε_b are the values at breaking point. The elastic modulus E was determined from the slope within the initial linear region (less than 10% strain) of the stress−strain curve. The work of extension W_b, a parameter to characterize the toughness of the sample, was calculated as the area under the stress−strain curve until fracture of the sample. All the samples were measured for at least three separate tests, and all the tensile properties were denoted by average value with standard deviation (error bar).

III. RESULTS AND DISCUSSION

Structure Optimization. Figure 1 shows the DIC images and the size distributions of microgels in various conditions.

dx.doi.org/10.1021/ma3003664 | Macromolecules 2012, 45, 5218−5228

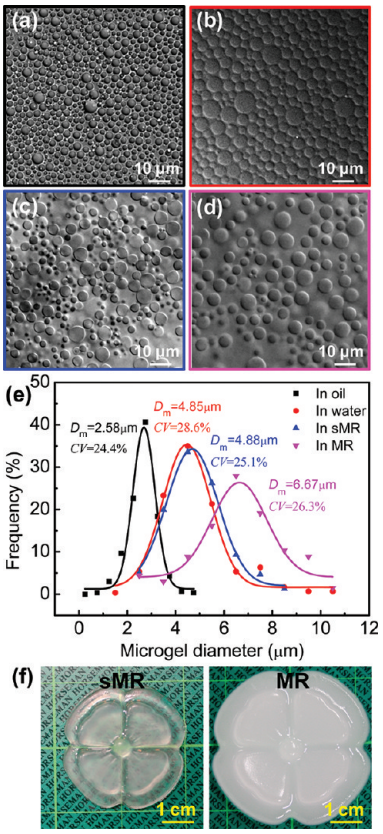

Figure 1. DIC optical micrographs of NaAMPS emulsion (a), PNaAMPS microgels swollen in water (b), PNaAMPS/PAAm microgels in swollen sMR0.07-4-(2-0.01) gel (c), and PNaAMPS/PAAm^2 microgels in swollen MR0.07-4-(2-0.01)-4 gel (d). The microgels in parts c and d were dyed by Alcian Blue to increase the visibility. (e) Size distributions of microgels determined from parts a–d. (f) Photographs of sMR0.07-4-(2-0.01) gel and MR0.07-4-(2-0.01)-4 gel.

The well-dispersed microgels with narrow size distributions can be observed qualitatively from Figure 1a–d. In general, these negatively charged microgels are very stable and they spontaneously redisperse in water after being freeze-dried. Benefitting from the good dispersibility of the microgels, we could statistically measure their diameters to obtain the size distributions from Figure 1a–d, as shown in Figure 1e. NaAMPS monomer emulsion in oil shows the mean diameter D_m of 2.58 μm, while water swollen PNaAMPS microgels show a notable increase in D_m of 4.85 μm, which is the result of the high osmotic pressure due to polymer strands and dissociated counterions in the microgels. PNaAMPS/PAAm microgels in swollen sMR0.07-4-(2-0.01) gel shows the comparable D_m with that of water-swollen PNaAMPS microgels, demonstrating the negligible osmotic pressure difference induced by the PAAm network between the inside and the outside of the microgels. D_m of PNaAMPS/PAAm^2 microgels in swollen MR0.07-4-(2-0.01)-4 gel largely increases to 6.67 μm, indicating the prominent effect of the osmotic pressure difference from the PAAm^2 network between the inside and the outside of the microgels. The variation of D_m for sMR and MR gels indicate that the PAAm concentration distribution in sMR gels is relatively uniform, while in MR gels the concentration is dilute in the matrix phase and dense in the microgel phase. The coefficient of variation CV of all the samples shows the similar value of ~26%, which indicates that the statistics based on the image analysis is reliable.

It should be emphasized that the microgels embedded in PAAm matrix without any treatment are quite difficult to identify, because highly swollen microgels have a refractive index close to that of water and scatter little light. Furthermore, the microgels in sMR gels are more ambiguous than those in MR gels under the DIC microscope, indicating the lower refractive index difference in and around the microgels in sMR gels, which is consistent with the result from the variation of D_m, and is also supported by the fact that sMR gels show the higher transparency than MR gels (Figure 1f). Therefore, we dyed the microgels with positively charged Alcian Blue in Figure 1c,d to increase the visibility.

As shown in Figure 2a, the appearance of the MR gel is quite turbid due to the two-phase composite structure, in contrast

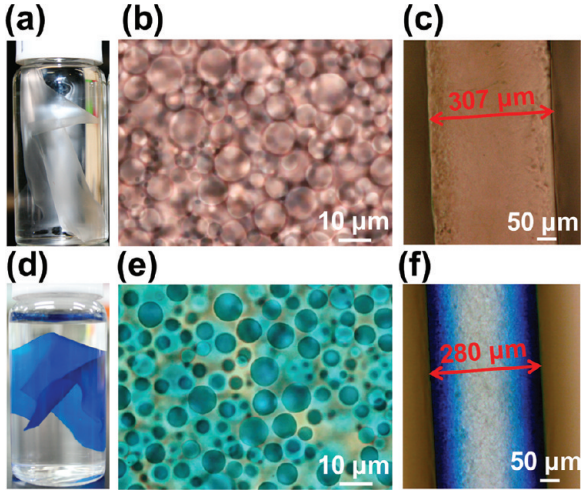

Figure 2. Photos and optical micrographs of MR gels (a, b, c) and Alcian Blue-dyed MR gels (d, e, f) in their fully swollen state. (a, d) Photos of the gel films; (b, e) views from the surface of the gels; (c, f) views from the cross-section of the gels. Sample formulation: MR0.07-4-(2-0.01)-4.

with conventional bicontinuous DN gels that are highly transparent. The microgels are difficult to identify from the background PAAm matrix under an optical microscope (Figure 2b), so we selectively dyed the anionic PNaAMPS of the PNaAMPS/PAAm^2 microgels with the tetravalent cationic Alcian Blue by electrostatic attraction, while the neutral PAAm matrix is still colorless (Figure 2e). Figure 2c,f present that the MR gel has very smooth surface and its thickness is homogeneous and thin, of ~300 μm, which favors the observation of the microgels. Moreover, Figure 2f shows that only the superficial layers of the MR gel are dyed with a gradient color along the thickness direction due to the diffusion and complexation of Alcian Blue with PNaAMPS.

As revealed in the previous work,[21] the microgels in MR gels act as multifunctional physical cross-linked points by interpenetrating with flexible PAAm matrix and serve as sacrificial bonds to reinforce MR gels. Therefore, increasing the PNaAMPS microgel concentration in the polymerization as much as possible should be favorable to the mechanical strength of MR gels. However, the viscosity of the precursor solution dramatically increases with the dried PNaAMPS microgel concentration $C_{microgel}$ due to the dramatic swelling of the polyelectrolyte microgels in water, which makes the

dx.doi.org/10.1021/ma3003664 | Macromolecules 2012, 45, 5218–5228

solution difficult to operate. The viscosity η of a colloid solution is related to the volume fraction of the colloid ϕ by the Einstein−Guth−Gold equation as $\eta = \eta_0(1 + 2.5\phi + 14.1\phi^2)$, where η_0 is the viscosity of water.[33] To avoid the high viscosity, we temporarily reduce the size of the swollen polyelectrolyte microgels by adding NaCl to the precursor solution. Therefore, we investigated the effect of NaCl concentration C_{NaCl} on the relative volume change of the microgels.

Figure 3a shows the image of volume change of PNaAMPS microgels (dried microgel concentration $C_{microgel}$ = 0.005 g/mL) in various C_{NaCl} solutions after sedimentation. The volume of the sedimentary PNaAMPS microgels decreases with the increase of C_{NaCl}. For ionic microgels, the dominating contributions to the free energy of swelling arise from the screened repulsion between polymer chains with fixed-charges and from the osmotic pressure exerted by the confined counterions. Therefore, with the addition of NaCl, the decrease in the volume of sedimentary microgels is the result of the shrinkage of microgels and intermicrogel spacing due to electrostatic screening. Figure 3b shows the relation between the volume ratio (V/V_0) and C_{NaCl} for the microgels, where V and V_0 are the sedimentation volume of microgels in C_{NaCl} solutions and in water, respectively. The result for the bulk PNaAMPS gel with the same chemical composition as the microgels is also presented in the figure. As shown in Figure 3b, with the increase of C_{NaCl}, V/V_0 decrease abruptly below 0.5 M of C_{NaCl} and tend to reach a constant above 0.5 M of C_{NaCl}. Comparing with the PNaAMPS bulk gel, the volume of PNaAMPS microgels decrease less substantially with the increase of C_{NaCl}, which indicates that intermicrogel spacing exists after the sedimentation.

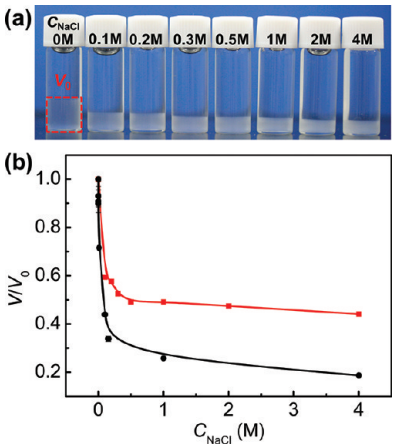

Figure 3. (a) Image of PNaAMPS microgels after sedimentation in aqueous solution of different NaCl concentration C_{NaCl}. (b) Volume ratio (V/V_0), as a function of C_{NaCl} for PNaAMPS microgels (red ■) and bulk PNaAMPS gel (●). For the case of PNaAMPS microgels, V_0 and V are corresponding to the volume of sedimentation microgels in pure water and in C_{NaCl} solutions, respectively, while for the case of bulk PNaAMPS gel, V_0 and V are corresponding to the swollen volume of bulk gel in pure water and in C_{NaCl} solutions, respectively. In this experiment, 0.01 g of dried PNaAMPS microgels were added in 2 mL of aqueous solution with different C_{NaCl}, and the colloidal solutions were left to stand for several days. The bulk PNaAMPS gel was synthesized from an aqueous solution of 1 M NaAMPS containing 4 mol % MBAA and 0.1 mol % OA, with the same formulation as the PNaAMPS microgels.

Although the effect of C_{NaCl} on the volume change of microgels is weak above 0.5 M, it still decreases the viscosity of microgels solution effectively, especially for the case of high $C_{microgel}$ reaching close packing state. This is due to a slight change in the volume fraction will prominently cause a change in the viscosity of the solution at a high volume fraction since the viscosity is dominated by the third nonlinear term of the Einstein−Guth−Gold equation.

The physical properties of MR gels were found to be strongly related to formulation parameters $C_{microgel}$, C_{NaCl}, C_{AAm1}, C_{MBAA1}, and C_{AAm2}. We first discussed the effects of $C_{microgel}$ on the mechanical behaviors of sMR and MR gels for constant C_{NaCl}, C_{AAm1}, C_{MBAA1}, and C_{AAm2}. With the increase of $C_{microgel}$, both sMR and MR gels show prominent enhancement in stiffness and strength, and transit from their corresponding PAAm gels to DN gels (Figure 4a,b). From Figure 4a,b, the fracture strain ε_b (Figure 4c) decreases, but fracture stress σ_b (Figure 4d), modulus E (Figure 4e), and work of extension W_b (Figure 4f) increase with $C_{microgel}$ for sMR and MR gels. Comparing with sMR gels, MR gels exhibit more superior mechanical properties. Figure 4 reveals that the addition of microgels can effectively improve the mechanical strength and toughness of soft PAAm gels, and the higher volume fraction of microgels embedded in the PAAm matrix will result in the higher mechanical strength and toughness.

The mechanical strength of sMR and MR gels decreases slightly with the increase of C_{NaCl} (Figure 5a,b). As shown in Figure 5c, with the increase of C_{NaCl}, sMR gels show the decreases in modulus E and turbidity τ, and increase in volume expansion ratio Q. Upon the addition of NaCl, less AAm is incorporated into the PNaAMPS microgels due to the shrinkage of the microgels, which leads to the weak interpenetrating entanglement of the polymerized PAAm matrix to the microgels and favors the swelling of sMR gels. Accordingly, the variations in E, Q, and τ for sMR gels with the increase of C_{NaCl} can be understood by the decreased volume fraction of the embedded microgels upon swelling. The decreases in E, Q, and τ for MR gels can also be explained by the decreased volume fraction of the microgels.

The mechanical strength of sMR and MR gels substantially increases with C_{AAm1} (Figure 5d,e). As shown in Figure 5f, with the increase of C_{AAm1}, sMR gels show the increase in E, but are insensitive in Q and τ, and MR gels show the increase in E and the decreases in Q and τ. On one hand, the high C_{AAm1} results in strong trapped entanglements between sparsely cross-linked PAAm matrix and densely cross-linked microgels, contributing to restrict the swelling. On the other hand, the high C_{AAm1} induces high osmotic pressure that is in favor of swelling. These two opposite effects make sMR gels insensitive in Q and τ. After the second PAAm polymerization, it is more difficult for MR gels prepared from higher C_{AAm1} to swell further.

C_{MBAA1} is a very important parameter for preparing tough MR gels. Brittle MR gels could be obtained even in the absence of cross-linker MBAA, indicating that the microgels embedded in the gels play a role in additional multifunctional physical cross-linked points. The mechanical strength of sMR and MR gels increases with C_{MBAA1} ranged from 0.01 mol % to 0.2 mol % (Figure 5g,h). As shown in Figure 5i, with the increase of C_{MBAA1}, sMR and MR gels show the increase in E and the decreases in Q and τ. All these results can be explained by the increased chemical cross-linking degree of the PAAm matrix.

Figure 5j shows the obvious decrease in σ_b and ε_b with the increase of C_{AAm2} for MR gels. In Figure 5k, with the increase of

dx.doi.org/10.1021/ma3003664 | Macromolecules 2012, 45, 5218−5228

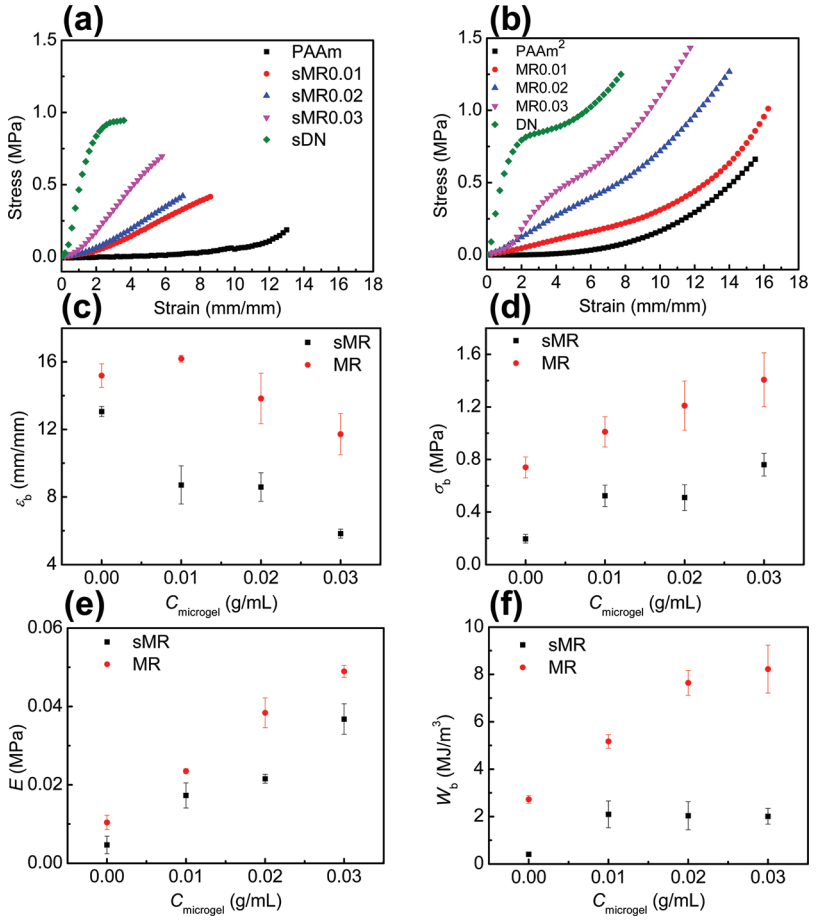

Figure 4. Effect of dried PNaAMPS microgel concentration $C_{microgel}$ on the tensile stress−strain curves of sMR $C_{microgel}$-0.1-(2-0.01) gels (a) and MR $C_{microgel}$-0.1-(2-0.01)-2 gels (b). PAAm 0-0-(2-0.01), PAAm^2 0-0-(2-0.01)-2, sDN, and DN gels are also shown in (a) and (b), respectively, for comparison. Dependences of fracture strain ε_b (c), fracture stress σ_b (d), modulus E (e), and work of extension W_b (f) on $C_{microgel}$ for sMR and MR gels.

C_{AAm2}, MR gels show the linear increases in E, Q, and τ. The effect of C_{AAm2} on Q and τ for MR gels is opposite to that of C_{NaCl}, C_{AAm1}, and C_{MBAA1}, which indicates that the osmotic pressure contribution of the second PAAm network surpasses the topological entanglement contribution.

Comparing with sMR gels (Figure 5a,d,g), MR gels (Figure 5b,e,h) show remarkable improvement in the tensile properties (ε_b of sMR and MR gels as a function of C_{NaCl}, C_{AAm1}, C_{MBAA1}, and C_{AAm2} are shown in Figure S1 of the Supporting Information). In Figure 5c,f,i, E of MR gels is higher than that of sMR gels, as a result of higher chain density and more permanently trapped entanglements, and τ of MR gels is also higher than that of sMR gels (one example is shown in Figure 1f). It is interesting that τ increases with Q for all the samples as shown in Figure 5c,f,i,k, which is different from traditional hydrogels with continuous phase. This abnormal phenomenon indicates that the transparency of MR gels is mainly influenced by light scattering on the interface between the PAAm matrix and DN microgels, which is related to the concentration difference of the PAAm polymer in and around the microgels. The more MR gels swell, the larger the concentration difference of the PAAm polymer is, which indicates that the PAAm network is dilute in the matrix phase and dense in the microgel phase. The latter is due to the confinement of the densely cross-linked PNaAMPS microgel networks.

To elucidate the correlation between the toughness and the strength of the gels, we plotted work of extension W_b (representation of toughness) and fracture stress σ_b (representation of strength) of all the samples in Figure 6a. We found that W_b and σ_b, roughly speaking, are linearly correlated, and they are simultaneously improved for MR gels in comparison with sMR gels. At the optimal formulation, MR gels exhibit superior mechanical properties, even exceed conventional DN gels prepared at the same formulation. For example, the MR0.075-4-(2-0.01)-4 gel shows E of 0.22 MPa, σ_b of 2.5 MPa, ε_b of 1300%, and W_b of 14 MJ/m^3, even with a high water content of 85%. The result of this gel is highlighted by the black arrow in Figure 6a. As shown in Figure 6b, the MR0.075-4-(2-0.01)-4 gel film with the thickness of 300 μm and the width of 2 mm can even bear 100 g load.

Both sMR gels and MR gels have a two-phase composite structure, where the disperse phase is the *rigid* double-network (DN) microgels, and the continuous phase is the *soft* PAAm matrix. To preferentially fracture the rigid and brittle PNaAMPS network in the microgels with the identical fracture mechanism of bulk DN gels, the PAAm network, both in the microgel phase and in the matrix phase, should have a fracture stress higher than the yield stress of the PNaAPMS network. According to the studies on bulk DN gels,[12] this condition is satisfied when the molar ratio of the PAAm to the PNaAMPS reaches the optimal value of 20−30. According to the volume

dx.doi.org/10.1021/ma3003664 | *Macromolecules* 2012, 45, 5218−5228

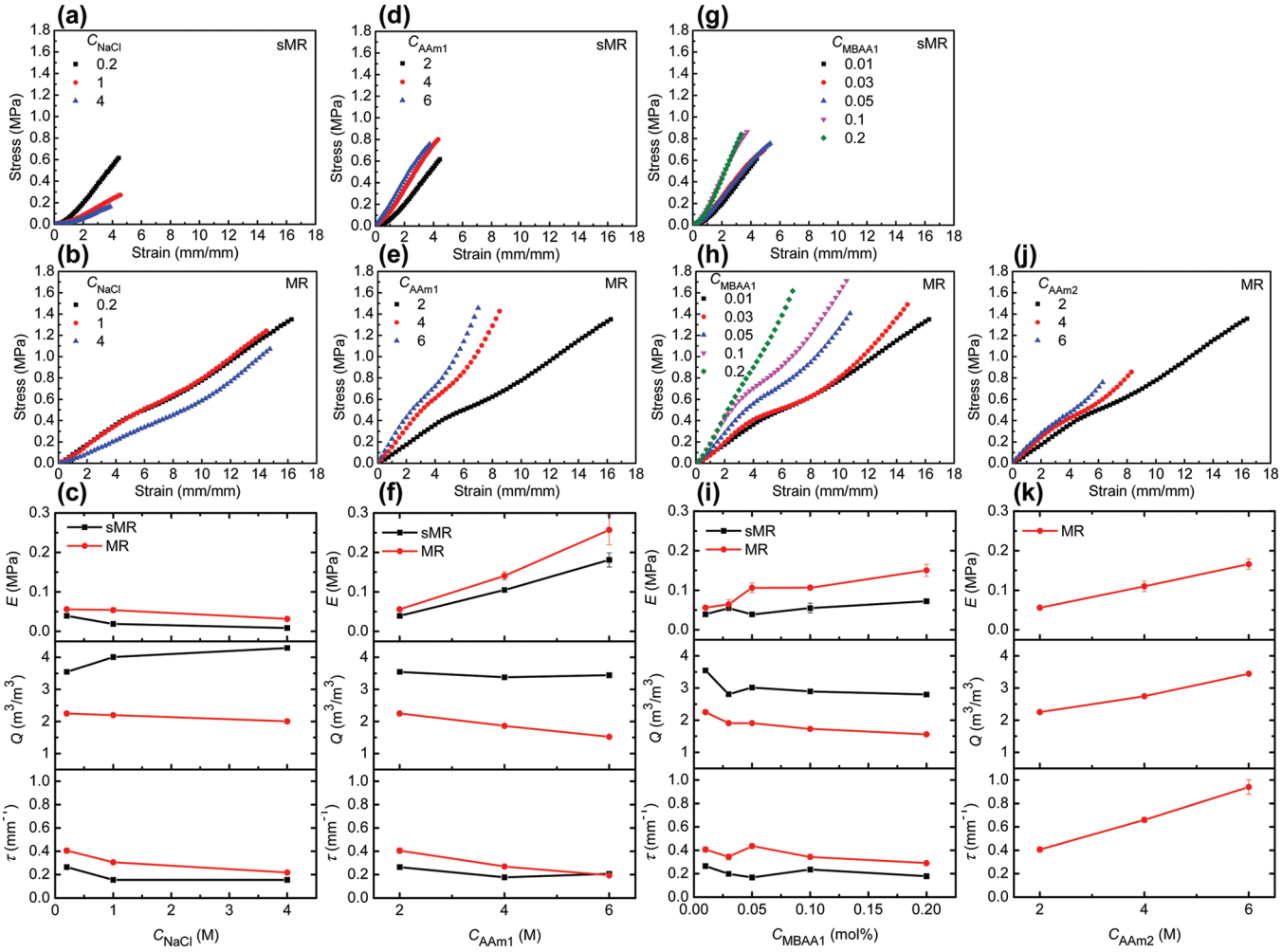

Figure 5. Effects of C_{NaCl} (a, b, c), C_{AAm1}(d, e, f), C_{MBAA1} (g, h, (i), and C_{AAm2} (j, k) on the tensile stress−strain curves of sMR and MR gels, as well as their physical properties (modulus E, volume expansion ratio Q, and turbidity τ). Sample formulation: (a) sMR 0.04-C_{NaCl}-(2-0.01); (b) MR 0.04-C_{NaCl}-(2-0.01)-2; (d) sMR 0.04-0.2-(C_{AAm1}-0.01); (e) MR 0.04-0.2-(C_{AAm1}-0.01)-2; (g) sMR 0.04-0.2-(2-C_{MBAA1}); (h) MR 0.04-0.2-(2-C_{MBAA1})-2; (j) MR 0.04-0.2-(2-0.01)-C_{AAm2}.

variation of the bulk PNaAMPS gel with C_{NaCl} (Figure 3b), we estimated that the molar ratio of the PAAm to the PNaAMPS in the microgels is about 4−9 in sMR gels prepared with C_{NaCl} ranged from 0.1 to 4 M, much lower than the optimal value of 20−30. With the introduction of the second PAAm network, this molar ratio increases to about 24−29 in MR gels, close to the optimal value. Actually, except for the cases of high $C_{microgel}$, the two-step sequential polymerization of PAAm network is not necessary to prepare tough MR gels; in the case of sMR0.01-0-(2-0.01) gel, it also achieved satisfactory tensile properties by only one-step polymerization of PAAm network, because the molar ratio of the PAAm to the PNaAMPS reached the optimal value after the first polymerization in the absence of NaCl. Thus, the molar ratio of the PAAm to the PNaAMPS in the microgels is the critical parameter to explain why MR gels exhibited more superior mechanical properties than sMR gels.

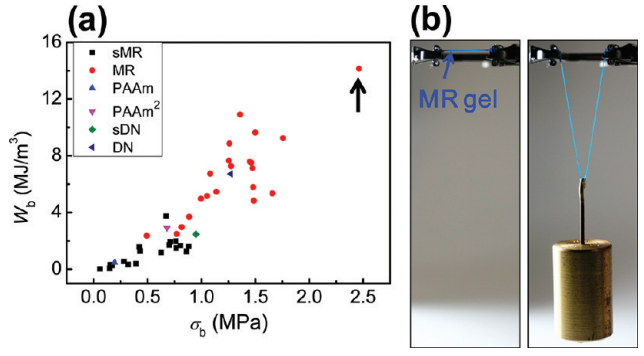

Figure 6. (a) Relationship between work of extension W_b and fracture stress σ_b for all the samples. The black arrow indicates the highest mechanical strength and toughness, which is the result of the sample with the optimal formulation, MR0.075-4-(2-0.01)-4. (b) Photos of dyed MR0.075-4-(2-0.01)-4 gel film (blue color) of 300 μm thickness and 2 mm width bearing no load (left) and bearing 100 g load (right).

Mechanical Model for the Two-Phase Structure. For elastic two-phase composites, two classic models are proposed by Voigt[34] and Reuss,[35] which give rigorous upper and lower bounds on the Young's modulus of composites, respectively. Over the last several decades, some other more complicated theoretical frameworks have been developed for predicting properties of composite materials, such as the composite theories of Mori−Tanaka,[36] Hapin−Tsai,[37] and Hashin−Shtrikman,[38] etc.

In this paper, we discuss whether the mechanical behaviors of the MR gels at *small* deformation can be described by the

dx.doi.org/10.1021/ma3003664 | Macromolecules 2012, 45, 5218−5228

simple isostrain model (Voigt's model) or isostress model (Reuss's model). In isostrain model, the strain field throughout the composite is assumed to be uniform and equal to that of an applied macro strain, whereas in isostress model, the stress field throughout the composite is assumed to be uniform and equal to that of an applied macro stress. The equations on the stress−strain relationship in isostrain model are given as follows:

$$\varepsilon = \varepsilon_1 = \varepsilon_2 \tag{4}$$

$$\sigma = \phi_1\sigma_1 + \phi_2\sigma_2 \tag{5}$$

$$E = \phi_1 E_1 + \phi_2 E_2 \tag{6}$$

The equations on the stress−strain relationship in isostress model are

$$\sigma = \sigma_1 = \sigma_2 \tag{7}$$

$$\varepsilon = \phi_1\varepsilon_1 + \phi_2\varepsilon_2 \tag{8}$$

$$\frac{1}{E} = \frac{\phi_1}{E_1} + \frac{\phi_2}{E_2} \tag{9}$$

where ε, σ, E, and ϕ represent strain, stress, Young's modulus, and volume fraction, respectively, and the parameters without subscript, with subscript 1, and with subscript 2 refer to the composite, filler phase, and matrix phase, respectively. $\phi_1 + \phi_2 = 1$.

Figure 7 shows that when MR0.07-4-(2-0.01)-4 gel was elongated to the ε of 100% (in the elastic region of MR gels),

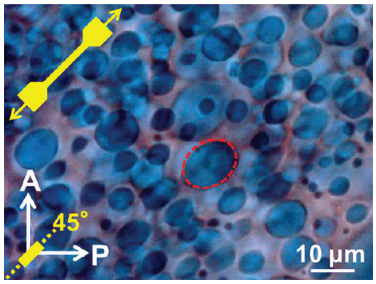

Figure 7. Real-time tensile observation of Alcian Blue-dyed MR0.07-4-(2-0.01)-4 gel at the strain ε of 100% under the polarizing microscope, equipped with the crossed polarizers and the 530 nm tint plate. The sample was stretched 45° against the polarizers. The red dashed circle indicates the deformed microgel. The strain of the deformed microgels ε_1 of 22% was the average of the strain of five microgels, determined from the major axis after and before deformation assuming that the volume of microgels was constant during elongation.

the microgels deformed from sphere to ellipsoid along with the stretching direction but showed a much smaller ε_1 of 22% than the applied macro strain ε on the MR gel. This fact indicates that isostrain model that assumes ε should be equal to ε_1 (eq 4) is not suitable for MR gels. Accordingly, we use isostress model to analyze the mechanical results of MR gels.

For two-phase composite sMR and MR gels, the volume fraction of microgels ϕ_1 is a very crucial parameter. As shown in Table 1, the ϕ_1 estimated from eq 3 increases with the increase of $C_{microgel}$ and the decrease of C_{NaCl}. The ϕ_1 of a MR sample is close to that of the associated sMR sample. In consideration of the increase in microgel diameter D_m of the MR gel in comparison with that of the associated sMR gel, as shown in Figure 1c and Figure 1d, this result indicates that the PAAm matrix phase and the microgel phase in MR gels swell to the

Table 1. Physical Characteristics of Various sMR and MR Gels

hydrogel	composition	Φ_1[a]	q (g/g)	E (MPa)	E_2[b] (MPa)
sMR gels	0-0-(2-0.01)	0	28.0	0.005	0.005
	0.01-0-(2-0.01)	0.042	16.7	0.025	0.024
	0.01-0.1-(2-0.01)	0.063	22.9	0.017	0.016
	0.01-0.5-(2-0.01)	0.057	26.2	0.009	0.008
	0.02-0.1-(2-0.01)	0.055	17.5	0.022	0.021
	0.03-0.1-(2-0.01)	0.119	13.9	0.037	0.033
	0.04-0.3-(2-0.01)	0.150	18.0	0.037	0.033
	0.06-1-(2-0.01)	0.319	17.6	0.051	0.039
	0.07-4-(2-0.01)	0.122	21.5	0.011	0.010
	0.075-4-(2-0.01)	0.265	20.3	0.049	0.039
MR gels	0-0-(2-0.01)-2	0	17.7	0.010	0.010
	0.01-0-(2-0.01)-2	0.095	10.9	0.036	0.033
	0.01-0.1-(2-0.01)-2	0.042	15.4	0.023	0.023
	0.01-0.5-(2-0.01)-2	0.031	13.2	0.021	0.020
	0.02-0.1-(2-0.01)-2	0.066	11.8	0.038	0.036
	0.03-0.1-(2-0.01)-2	0.088	10.7	0.049	0.045
	0.04-0.3-(2-0.01)-2	0.153	10.4	0.065	0.057
	0.06-1-(2-0.01)-2	0.245	11.1	0.068	0.054
	0.07-4-(2-0.01)-4	0.182	7.7	0.131	0.115
	0.075-4-(2-0.01)-2	0.243	9.1	0.119	0.099
	0.075-4-(2-0.01)-4	0.306	6.7	0.215	0.185

[a] ϕ_1 was estimated from eq 3. [b] E_2 was calculated by eq 9. E_1 of sMR gels and MR gels were estimated from the modulus of the sDN gel and DN gel with the similar formulation to the embedded microgels in sMR and MR gels, respectively. $E_{1,sMR} \approx E_{sDN} = 0.16$ MPa, $E_{1,MR} \approx E_{DN} = 0.34$ MPa.

similar extent after the second PAAm polymerization, so that the volume fraction ϕ_1 keeps constant.

Assuming that the isostress model is applicable, we estimated E_2 from ϕ_1, E, and E_1 by using eq 9, where the modulus of DN microgels E_1 was approximately estimated from the measurement of the DN gel with the similar formulation, and the results are shown in Table 1. Comparing the measured E with the calculated E_2 in Table 1, we found that E approximately equals to E_2 at the low ϕ_1 ($\phi_1 < 10\%$) and is much larger than E_2 at the high ϕ_1 ($\phi_1 > 10\%$), which means that the stiff microgels do not play a notable role in E until ϕ_1 reaches an appropriate value of about 10%. We also found that the modulus of the matrix PAAm phase, E_2, increases with ϕ_1, which indicates the confined swelling of PAAm matrix due to the additional physical cross-links upon interpenetrations and entanglements with the microgels. This conjecture is supported by the decrease in the swelling ratio q with the increase in ϕ_1. Therefore, on one hand, the increase in E with ϕ_1 is due to the incorporation of the relatively rigid microgels ($E_{1,sMR} = 0.16$ MPa and $E_{1,MR} = 0.34$ MPa). On the other hand, the increased E with ϕ_1 also results from the increased effective elastic chain density due to the topologically constrained chain entanglements between interpenetrating chains of the matrix and those of the microgels.

We further correlate the modulus E_2 and the swelling ratio q_2 of the fully swollen PAAm matrix quantitatively. Since q_2 could not be measured directly, we assume q_2 approximately equals to the overall swelling ratio of the gel, q, due to the rather low ϕ_1. In terms of the Flory−Rehner theory,[39] the shear modulus G and equilibrium swelling ratio q of a fully swollen neutral gel is related by scaling relationships.[40]

dx.doi.org/10.1021/ma3003664 | Macromolecules 2012, 45, 5218−5228

$$G(1/q) \approx \frac{kT}{b^3}\begin{cases} q^{-2.25} & T \gg \theta \\ q^{-3} & T = \theta \end{cases} \quad (10)$$

Here, k is the Boltzmann constant, T is the absolute temperature, θ is the θ-temperature, and b is the Kuhn length. The cases of $T \gg \theta$ and $T = \theta$ correspond to good solvent and θ-solvent, respectively.

Figure 8 shows the dependences of E_2 on q in a double logarithmic coordinate for sMR and MR gels listed in Table 1.

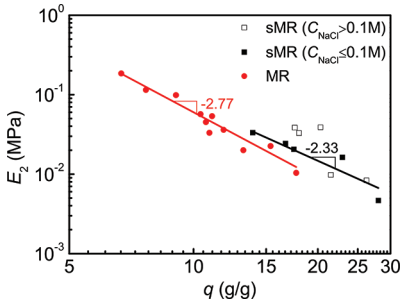

Figure 8. Dependences of modulus of fully swollen PAAm matrix E_2 on equilibrium swelling ratio q for sMR and MR gels listed in Table 1. The black line is the least-squares regression fit for sMR gels prepared at $C_{NaCl} \leq 0.1$ M, and the red line is the least-squares regression fit for MR gels. The numbers are the slopes of the lines.

We found that all the data of MR gels as well as the data of sMR gels prepared at the low C_{NaCl} ($C_{NaCl} \leq 0.1$ M) fit a power law ($E_2 \sim q^{-x}$). Though, some of the data of sMR gels prepared at the high C_{NaCl} ($C_{NaCl} > 0.1$ M) deviated from the power law; which probably originates from the fact that some microgels aggregate when $C_{NaCl} > 0.1$ M and the microgels are no longer uniformly distributed in the PAAm matrix. The least-squares regression fits give the scaling exponent $x = 2.33$ for sMR gels ($C_{NaCl} \leq 0.1$ M) and $x = 2.77$ for MR gels, both of which are in the range $2.25 < x < 3$ given by eq 10, which is consistent with the fact that the Flory–Huggins interaction parameter χ of PAAm in water is 0.45, very close to the θ-solvent of 0.5.[41] The slightly larger x of MR gels than that of sMR gels indicates that the water deteriorates toward θ conditions after the introduction of the second PAAm network. The early researches also claim that x for PAAm hydrogels increases from 2.25 to 3.1 with the increase of C_{MBAA1} from 0 to 3.25 mol %.[42,43]

Because the scaling relationships between E_2, estimated from the isostress model, and q are in reasonable agreement with the Flory–Rehner theory, the isostress model is suitable for sMR and MR gels.

Structural Picture. There is no doubt that the excellent mechanical performances of MR gels have significant connection with their two-phase composite structure, where the disperse phase is the DN microgels and the continuous phase is the lightly cross-linked PAAm matrix. The diameter D_m of the microgels in sMR and MR gels have been characterized as about 5 and 7 μm, respectively (Figure 1). If we assume that the length of a carbon–carbon bond is ~0.1 nm, the contour length of a network strand in sMR gels can be estimated as ~1 μm through multiplying the bond length by the average carbon–carbon bond number N of a strand (in the case of C_{MBAA1} = 0.01 mol %, N is estimated as 10^4), which is of the same order of magnitude of the microgels. If we consider that the polymer strands of the PAAm matrix are in Gaussian distribution, their modulus E_2 can be described by the rubber elasticity theory,

$$E_2 = 3\nu_e kT \quad (11)$$

where ν_e is the number of elastic entanglement strands per unit volume, k is the Boltzmann constant, and T is the absolute temperature. Further, each elastic entanglement strand can be described as a blob with the correlation length ξ, which is taken to represent the mesh size of the polymer network.

$$\frac{1}{\nu_e} = \frac{4}{3}\pi\left(\frac{\xi}{2}\right)^3 \quad (12)$$

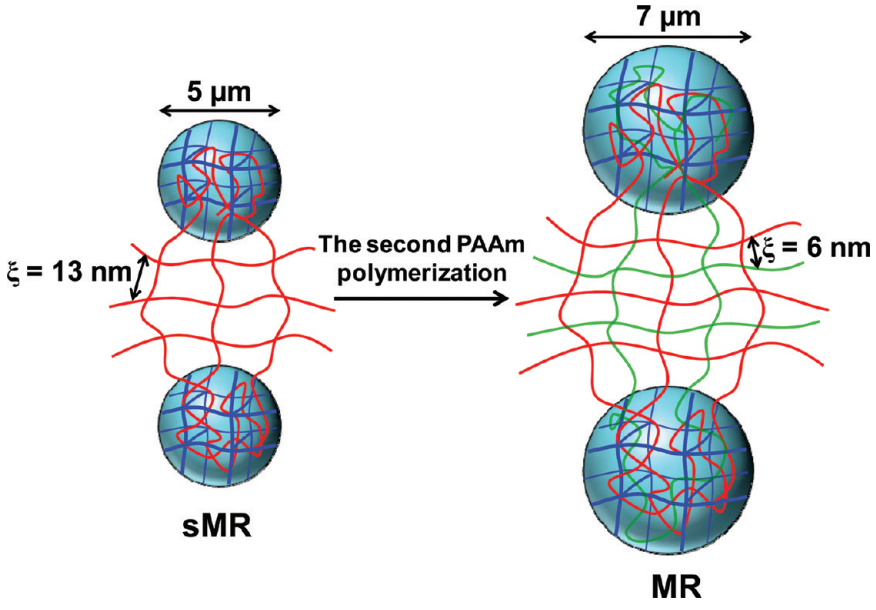

Figure 9. Schematic representation of the structure of sMR gels and MR gels. The first and the second PAAm network are represented in red and in green for clarity, respectively. The values of the mesh size ξ in the figure are estimated for sMR0.07-4-(2-0.01) gel and MR0.07-4-(2-0.01)-4 gel.

dx.doi.org/10.1021/ma3003664 | Macromolecules 2012, 45, 5218–5228

Therefore, we calculated ξ = 13 nm for sMR0.07-4-(2-0.01) gel and ξ = 6 nm for MR0.07-4-(2-0.01)-4 gel by eqs 11 and 12, respectively, from their modulus E_2 measured at room temperature.

Because of the extremely low C_{MBAA1}, the major contribution to the modulus of PAAm matrix is dominated consequentially by the physical entanglements acting as additional cross-linked junctions. Comparing with the pure PAAm network, the introduction of the second PAAm network and the highly cross-linked PNaAMPS microgels working as multifunctional physical cross-linked points in MR gels intensifies the extent of entanglements highly. In fact, the PAAm matrix in the vicinity of the microgels should possess higher chain density and entanglements than that far away from the microgels, as a result of the confined swelling. A high surface fraction of the microgels will result in the high modulus of MR gels. We define S as the microgel surface area in unit volume,

$$S = 4\pi R_m^{\ 2} \times \frac{\phi_1}{\frac{4}{3}\pi R_m^{\ 3}} = \frac{3\phi_1}{R_m} \tag{13}$$

which is proportional to ϕ_1 and inversely proportional to R_m (mean radius of microgels). This relation has been confirmed by the results shown in Table 1 and Figure 8, which show that the high ϕ_1 leads to the high modulus for the same R_m. Eq 13 also indicates that the high modulus of MR gels will be attained if microgels with the small R_m are used for the same ϕ_1.

VI. CONCLUSIONS

Microgel-reinforced hydrogels with high mechanical strength and toughness, MR hydrogels, have been successfully fabricated by salt-controlled swelling of highly cross-linked anionic PNaAMPS microgels (D_m: ~5 μm, CV: ~26%) and two-step sequential UV polymerization of lightly cross-linked neutral PAAm networks. For the complicated systems, we have investigated the effects of $C_{microgel}$, C_{NaCl}, C_{AAm1}, C_{MBAA1}, and C_{AAm2} on the mechanical behaviors of sMR and MR gels, and have found that MR0.075-4-(2-0.01)-4 gel is the optimal formulation in terms of the mechanical strength and toughness. The same as bulk DN gels, the molar ratio of the PAAm to the PNaAMPS in the microgels is the most crucial parameter for the enhancement of the mechanical strength and toughness of MR gels and shall reach the optimal value of 20−30.

Further, we give a two-phase composite picture from the structural and mechanical viewpoints, as shown in Figure 9. Each microgel acts as a "cage" to restrict the swelling of PAAm network within the microgels, which results in the significant PAAm concentration difference inside and around the microgels, that is dense in the microgel phase and dilute in the matrix phase. The increase in the modulus of MR gels is a result of the addition of relatively rigid microgels, as well as the introduction of topologically constrained chain entanglements between interpenetrating chains of the matrix and those of the microgels.

On the basis of the fact that the local strain of microgels is far smaller than the global strain of MR gels, we conclude that isostress model (Reuss's model) is more suitable for MR gels than isostrain model (Voigt's model). The E_2 estimated from isostress model and q show a power law ($E_2 \sim q^{-x}$) with the scaling exponent of x = 2.33 for sMR gels and x = 2.77 for MR gels, both of which are in the range 2.25 < x < 3 predicted by the Flory−Rehner theory. The good agreement with the Flory−Rehner theory, in turn, also demonstrates the applicability of isostress model to sMR and MR gels.

Owing to the high mechanical strength and the visualization of the embedded microgels, these MR gels will be good model systems for the study of reinforcement mechanism in composite. Furthermore, it is quite interesting to pursue fracture mechanism of MR gels upon elongation in depth at the molecular level.

■ ASSOCIATED CONTENT

Supporting Information

Fracture strain ε_b of sMR and MR gels as a function of C_{NaCl}, C_{AAm1}, C_{MBAA1}, and C_{AAm2}. This material is available free of charge via the Internet at http://pubs.acs.org/.

■ AUTHOR INFORMATION

Corresponding Author

*E-mail: gong@mail.sci.hokudai.ac.jp.

Notes

The authors declare no competing financial interest.

■ ACKNOWLEDGMENTS

This research was financially supported by a Grant-in-Aid for Specially Promoted Research (No. 18002002) from the Ministry of Education, Science, Sports and Culture of Japan.

■ REFERENCES

(1) Hoffman, A. S. *Adv. Drug Deliver. Rev.* **2002**, *43*, 3.
(2) Lee, K. Y.; Mooney, D. J. *Chem. Rev.* **2001**, *101*, 1869.
(3) Yasuda, K.; Kitamura, N.; Gong, J. P.; Arakaki, K.; Kwon, H. J.; Onodera, S.; Chen, Y. M.; Kurokawa, T.; Kanaya, F.; Ohmiya, Y.; Osada, Y. *Macromol. Biosci.* **2008**, *9*, 307.
(4) Gong, J. P.; Katsuyama, Y.; Kurokawa, T.; Osada, Y. *Adv. Mater.* **2003**, *15*, 1155.
(5) Okumura, Y.; Ito, K. *Adv. Mater.* **2001**, *13*, 485.
(6) Haraguchi, K.; Takehisa, T. *Adv. Mater.* **2002**, *14*, 1120.
(7) Waters, D. J.; Engberg, K.; Parke-Houben, R.; Hartmann, L.; Ta, C. N.; Toney, M. F.; Frank, C. W. *Macromolecules* **2010**, *43*, 6861.
(8) Sakai, T.; Matsunaga, T.; Yamamoto, Y.; Ito, C.; Yoshida, R.; Suzuki, S.; Sasaki, N.; Shibayama, M. *Macromolecules* **2008**, *41*, 5379.
(9) Kaneko, T.; Tanaka, S.; Ogura, A.; Akashi, M. *Macromolecules* **2005**, *38*, 4861.
(10) Haque, M. A.; Kamita, G.; Kurokawa, T.; Tsujii, K.; Gong, J. P. *Adv. Mater.* **2010**, *22*, 5110.
(11) Huang, T.; Xu, H. G.; Jiao, K. X.; Zhu, L. P.; Brown, H. R.; Wang, H. L. *Adv. Mater.* **2007**, *19*, 1622.
(12) Gong, J. P. *Soft Matter* **2010**, *6*, 2583.
(13) Mayumi, K.; Ito, K. *Polymer* **2010**, *51*, 959.
(14) Haraguchi, K. *Curr. Opin. Solid State Mater. Sci.* **2007**, *11*, 47.
(15) Naficy, S.; Brown, H. R.; Razal, J. M.; Spinks, G. M.; Whitten, P. G. *Aust. J. Chem.* **2011**, *64*, 1007.
(16) Imran, A. B.; Seki, T.; Takeoka, Y. *Polym. J.* **2010**, *42*, 839.
(17) Yu, Q. M.; Tanaka, Y.; Furukawa, H.; Kurokawa, T.; Gong, J. P. *Macromolecules* **2009**, *42*, 3852.
(18) Brown, H. R. *Macromolecules* **2007**, *40*, 3815.
(19) Tanaka, Y. *Europhys. Lett.* **2007**, *78*, 56005.
(20) Saito, J.; Furukawa, H.; Kurokawa, T.; Kuwabara, R.; Kuroda, S.; Hu, J.; Tanaka, Y.; Gong, J. P.; Kitamura, N.; Yasuda, K. *Polym. Chem.* **2011**, *2*, 575.
(21) Hu, J.; Hiwatashi, K.; Kurokawa, T.; Liang, S. M.; Wu, Z. L.; Gong, J. P. *Macromolecules* **2011**, *44*, 7775.
(22) Haque, M. A.; Kurokawa, T.; Kamita, G.; Gong, J. P. *Macromolecules* **2011**, *44*, 8916.
(23) Aleman, J.; Chadwick, A. V.; He, J.; Hess, M.; Horie, K.; Jones, R. G.; Kratochvil, P.; Meisel, I.; Mita, I.; Moad, G.; Penczek, S.; Stepto, R. F. T. *Pure Appl. Chem.* **2007**, *79*, 1801.

(24) Huang, T.; Xu, H. G.; Jiao, K. X.; Zhu, L. P.; Brown, H. R.; Wang, H. L. *Adv. Mater.* **2007**, *19*, 1622.
(25) Qin, X. P.; Zhao, F.; Liu, Y. K.; Wang, H. Y.; Feng, S. Y. *Colloid Polym. Sci.* **2009**, *287*, 621.
(26) Jha, A. K.; Manisha, S. M.; Farach-Carson, M. C.; Duncan, R. L.; Jia, X. *Soft Matter* **2010**, *6*, 5045.
(27) Lally, S.; Liu, R.; Supasuteekul, C.; Saunders, B. R.; Freemont, T. *J. Mater. Chem.* **2011**, *21*, 17719.
(28) Liang, S. M.; Wu, Z. L.; Hu, J.; Kurokawa, T.; Yu, Q. M.; Gong, J. P. *Macromolecules* **2011**, *44*, 3016.
(29) Nisisako, T. *Chem. Eng. Technol.* **2008**, *31*, 1091.
(30) Erbil, C.; Sarac, A. S. *Eur. Polym. J.* **2002**, *38*, 1305.
(31) Litvinov, V. M.; Orza, R. A.; Klppel, M.; van Duin, M.; Magusin, P. C. M. M. *Macromolecules* **2011**, *44*, 4887.
(32) Lin, W. C.; Fan, W.; Marcellan, A.; Hourdet, D.; Creton, C. *Macromolecules* **2010**, *43*, 2554.
(33) Guth, E.; Gold, O. *Phys. Rev.* **1938**, *53*, 322.
(34) Voigt, W. *Wied. Ann.* **1889**, *38*, 573.
(35) Reuss, A. *Z. Angew. Math. Mech.* **1929**, *9*, 49.
(36) Mori, T.; Tanaka, K. *Acta Metall.* **1973**, *21*, 571.
(37) Halpin, J. C.; Kardos, J. L. *Polym. Eng. Sci.* **1976**, *16*, 344.
(38) Hashin, Z. *J. Appl. Mech.* **1983**, *50*, 481.
(39) Flory, P. J.; Rehner, J. *J. Chem. Phys.* **1943**, *11*, 521.
(40) Obukhov, S. P.; Rubinstein, M.; Colby, R. H. *Macromolecules* **1994**, *27*, 3191.
(41) Tominaga, T.; Tirumala, V. R.; Lee, S.; Lin, E. K.; Gong, J. P.; Wu, W. L. *J. Phys. Chem. B* **2008**, *112*, 3903.
(42) Cohen, Y.; Ramon, O.; Kopelman, I. J.; Mizrahi, S. *J. Polym. Sci., Part B: Polym. Phys.* **1992**, *30*, 1055.
(43) Mallam, S.; Horkay, F.; Hecht, A. M.; Geissler, E. *Macromolecules* **1989**, *22*, 3356.